Journal of Hazardous Materials 306 (2016) 295–304

Contents lists available at ScienceDirect

Journal of Hazardous Materials

journal homepage: www.elsevier.com/locate/jhazmat

Enhanced photocatalytic degradation of norfloxacin in aqueous Bi_2WO_6 dispersions containing nonionic surfactant under visible light irradiation

Lin Tang[a,b,*], Jiajia Wang[a,b], Guangming Zeng[a,b,*], Yani Liu[a,b], Yaocheng Deng[a,b], Yaoyu Zhou[a,b], Jing Tang[a,b], Jingjing Wang[a,b], Zhi Guo[a,b]

[a] College of Environmental Science and Engineering, Hunan University, Changsha 410082, PR China
[b] Key Laboratory of Environmental Biology and Pollution Control (Hunan University), Ministry of Education, Changsha 410082, PR China

HIGHLIGHTS

- TX100 strongly enhanced the adsorption and photodegradation of NOF in Bi_2WO_6 dispersions under visible light irradiation (400–750 nm).
- Cu^{2+} (10 mM) significantly suppressed the photocatalytic degradation of NOF.
- FT-IR demonstrated that the NOF adsorbed on Bi_2WO_6 was completely degraded.
- Three possible photocatalytic degradation pathways of NOF were proposed, according to the HPLC/MS/MS analysis.

ARTICLE INFO

Article history:
Received 28 September 2015
Received in revised form 2 December 2015
Accepted 22 December 2015
Available online 29 December 2015

Keywords:
Norfloxacin
Surfactant
Photocatalytic degradation
Visible light irradiation
Reaction mechanism

ABSTRACT

Photocatalytic degradation is an alternative method to remove pharmaceutical compounds in water, however it is hard to achieve efficient rate because of the poor solubility of pharmaceutical compounds in water. This study investigated the photodegradation of norfloxacin in a nonionic surfactant Triton-X100 (TX100)/Bi_2WO_6 dispersion under visible light irradiation (400–750 nm). It was found that the degradation of poorly soluble NOF can be strongly enhanced with the addition of TX100. TX100 was adsorbed strongly on Bi_2WO_6 surface and accelerated NOF photodegradation at the critical micelle concentration (CMC = 0.25 mM). Higher TX100 concentration (>0.25 mM) lowered the degradation rate. In the presence of TX100, the degradation rate reached the maximum value when the pH value was 8.06. FTIR analyses demonstrated that the adsorbed NOF on the catalyst was completely degraded after 2 h irradiation. According to the intermediates identified by HPLC/MS/MS, three possible degradation pathways were proposed to include addition of hydroxyl radical to quinolone ring, elimination of piperazynilic ring in fluoroquinolone molecules, and replacement of F atoms on the aromatic ring by hydroxyl radicals.

1. Introduction

The increasing antibiotic resistance of microorganism and antibiotic resistance in human body aroused by the presence of antibiotics in natural water gains great public attention [1]. Many antibiotics detected in aquatic environment, even at trace levels, may cause antibiotic resistance and lead to an adverse effect to aquatic wildlife, the ecosystem and human health [2,3]. Fluoroquinolones (FQs) is one of the most consumed antibiotics and has a total consumption of about 44 million kilograms every year in the world [4]. Norfloxacin (NOF), a second generation synthetic FQs, is widely used in veterinary medicine and treatment of human infections. Three of the primary sources of antibiotics entering the environment are medicine, agriculture, and pharmaceutical industry. Because a large portion of the administered doses are excreted, a substantial amount of NOF is released to the environment. NOF has poor solubility in water and easily deposits on aquatic sediments and soil. Thus, its environmental occurrence, transfer, fate, and potential risk during water treatment should be the focus of our concern.

Among the removal technologies of heavy metals and FQs from water, including adsorption, biological treatment, and advanced oxidation/reduction process (AO/RP) [5–11], AO/RP has been

* Corresponding authors at: College of Environmental Science and Engineering, Hunan University, Changsha 410082, PR China. Fax: +86 731 88822778.
E-mail addresses: tanglin@hnu.edu.cn (L. Tang), zgming@hnu.edu.cn (G. Zeng).

http://dx.doi.org/10.1016/j.jhazmat.2015.12.044
0304-3894/

proved to be a highly efficient and low cost method, and received considerable attention. AO/RP with the highly reactive hydroxyl radical (•OH), hydrated electrons (e_{aq}) and hydrogen atoms (H•) as main active species can effectively degrade these soluble biorefractory antibiotics [6]. The widely used photocatalyst, namely TiO_2, can mainly be excited by light in the ultraviolet region during oxidation process [12]. However, the exciting light in the UV region only accounts for 4% of the solar light in the complete spectrum of sunlight, which significantly limits the application of TiO_2 in photocatalysis. Bismuth tungstate (Bi_2WO_6) was reported to have an excellent photodegradation efficiency under visible light (400–800 nm) [13–16]. In previous studies, Bi_2WO_6 prepared by hydrothermal method displayed a certain photocatalytic activity capacity to NOF and Rhodamine under simulated solar light irradiation [17–21]. However, the poor solubility of NOF in aquatic environment limits the photocatalytic capacity to NOF.

In recent years, the use of surfactant solutions in prior extraction/washing steps for removal of organic contaminants from solid phases has been largely applied in sediment or soil remediation. It also gives a particular insight into potential use of dissolved surfactants in the photocatalysis treatment of complex poorly soluble pollutant in aqueous solution.

It should be noted that some surfactants can be completely decomposed by photocatalysis [22], so theoretically, they can compete with the target substrate for active sites on the semiconductor surface and thus retard the degradation of contaminants. Pramauro et al. indicated that the degradation of some aromatic pollutants in the presence of surfactants bearing alkyl chains is possible, although at relatively low reaction rates [23,24]. The possible beneficial effects arising from adsorption of surfactants onto the semiconductor surface were examined [25,26]. Hidaka et al. proposed the use of amphiphiles in photocatalysis and their resistance to radical attack and found that different types of surfactants have various effects on the photocatalytic process [27], depending on the pollutant hydrophobicity, solution pH, and surfactant concentration. Although the addition of surfactants will compete with the target pollutant for active sites on the catalyst, the degradation of poorly soluble substances can be strongly enhanced with the formation of surfactants micelle in aqueous solution. It was reported that introduction of anionic surfactant in TiO_2 dispersions induces the aggregation of cationic dyes, allowing the poorly soluble dye adsorbed on the photocatalyst surface, which strongly accelerated the photodegradation under visible light irradiation [28–30]. However, the specific mechanism of the complex system still remains unknown. What is more, many researchers have investigated the degradation pathway of pharmaceuticals in biological treatment and UV light treatment, but few researchers paid attention to the degradation intermediates during the visible light treatment [31,32]. It is necessary to investigate the efficiency of photocatalysis in degradation of antibiotics, such as NOF, in presence of surfactants under visible light. The degradation pathway and products of the pharmaceuticals during photo treatment process under visible light should also be our concern.

Triton X-100 (TX100), a nonionic surfactant, is capable of solubilizing hydrophobic contaminants that are relatively water insoluble. Previous study confirmed that TX100 was effective in removing polycyclic aromatic hydrocarbons and benzoapyrene from soils [33,34]. Besides, nonionic surfactants are preferable to anionic and cationic surfactants due to the following reasons: (1) They are less nontoxic [35]. (2) They are easily biodegradable and purchased [36]. We conducted this study to evaluate the feasibility of the photocatalytic decomposition of the target NOF by Bi_2WO_6 in surfactant micelles (TX100) and the impacts of the following coexisting substances on the photocatalytic degradation of NOF by Bi_2WO_6: inorganic anions (SO_4^{2-}, NO_3^-, and HCO_3^-) and inorganic cations (K^+, Ca^{2+}, Cu^{2+}, and Mg^{2+}). Fourier-transform infrared (FTIR) spectroscopy was used to determine whether the adsorbed NOF on the catalyst was degraded. Furthermore, photodegradation products during the treatment process and pathways of photocatalytic degradation of NOF were also investigated.

2. Materials and methods

2.1. Reagents

Norfloxacin ($C_{16}H_{18}FN_3O_3$, purity 99.8%) was purchased from Aladdin-Reagent Company, Shanghai. Triton X-100 were purchased from Aldrich Chemical Co., Ltd. Bismuth tungstate was synthesized using bismuth nitrate pentahydrate ($Bi(NO_3)_3{\cdot}5H_2O$) and sodium tungstate dihydrate ($Na_2WO_4{\cdot}2H_2O$) as precursors, which were purchased from Chemical Technology Co., Ltd., Tianjin, China. The preparation method is illuminated in Supplementary material. The salts including sodium sulfate (Na_2SO_4), sodium nitrate ($NaNO_3$), sodium bicarbonate ($NaHCO_3$), potassium chloride (KCl), magnesium chloride ($MgCl_2$), copper sulfate pentahydrate ($CuSO_4{\cdot}5H_2O$) and calcium chloride ($CaCl_2$) were obtained from Chemical Technology Co., Ltd., Tianjin, China. The mobile phase solvent for HPLC analysis (i.e., acetonitrile, formic acid) came from Tedia Company. All other reagents were of analytical purity. Solutions were prepared with high-purity water (18.25 M cm^{-1}) from a Milli-Q water purification system.

2.2. Surface tension measurements

The CMC for the TX100 containing systems was measured according to the Wilhelmy plate method using an interfacial tensiometer (Tensiometer K14 Krüss, Germany), and were performed in the absence and the presence of Bi_2WO_6. The mean value of the five measurements set at a temperature of 25 ± 1 °C was accepted as a result.

2.3. Photocatalytic degradation

Typically, photocatalytic degradation was performed in an aqueous Bi_2WO_6 suspension prepared by mixing 100 mg Bi_2WO_6 powder with 100 mL of solutions containing NOF and TX100 at an appropriate concentration. Prior to irradiation, the suspensions were stirred in the dark for 30 min to achieve the adsorption–desorption equilibrium. The light source, which was 300 W Xe lamp (CEL-HXF300 AULTT, Beijing, China) with a 400 nm cut off filter. At regular irradiation time intervals, 2 mL reaction solution was withdrawn and filtered through 13 mm × 0.45 μm membrane for NOF analysis.

2.4. Characterizations

FTIR spectra were obtained using a spectrometer (Spectrum GX, PerkinElmer, USA) within the 4000–400 cm^{-1} region at a 4 cm^{-1} resolution. About 2 mg of the milled sample was ground with 200 mg of KBr (FTIR grade) and compressed into a pellet under a vacuum at a pressure of 75 KN cm^{-2} for 3 min.

Crystallographic information of Bi_2WO_6 was obtained by X-ray diffraction (XRD, 43 Rigaku D/MAX-RB, Cu Kα radiation, Japan). The data were collected in the 20–80° 2θ range with 0.4° steps and a counting time of 5 s per step.

UV–vis diffused reflectance spectra (DRS, Shimadzu, UV-3150, Japan) of Bi_2WO_6 were obtained on a Hitachi U-3010 spectrometer, using $BaSO_4$ as the reference.

2.5. Analytical determination

The photodegradation products and intermediates of NOF were analyzed by HPLC (Agilent 1100). The determination of NOF and TX100 in the filtrates was performed using HPLC with the UV detector at 280 nm for NOF and 220 nm for TX100 under the following conditions: Kromasil C18 column, 250 × 4.6 mm i.d., at 25 °C. The mobile phase was 70:30(v/v) acetonitrile (CH_3CN) and formic acid solution (0.1% HCOOH); flow rate was 1 mL min^{-1}. For LC–MS/MS, an Agilent high-performance liquid chromatography (HPLC) system with the C18 column, 100 × 4.6 mm, 1290 auto sampler, 1290 Bin pumps, and API 3000 mass analyzer was used. LC separations were performed at the flow rate of 0.2 mL min^{-1} with injection volumes of 10 μL. The linear gradient elution was selected as the following: from 90% A (0.1% formic acid solution) and 10% B (CH_3CN) to 10% A and 90% B within 30 min and then reverse to the initial conditions within 10 min. An electrospray interface (ESI) was used for the MS and MS–MS measurements in positive ionization mode at the full scan acquisition between *m*/*z* 100–600. The collision energy varied according to the requirements for different measurements, and the other parameters were set as the following: the ESI was set as 4 kV, and the temperature was 400 °C. The gas (N_2) flow rate was 11 L min^{-1}, and nebulizer was 15 psi. Nitrogen was used as a collision gas at 2500 mbar.

2.6. Acute toxicity evaluation

The toxicity tests of NOF and its intermediates on *Escherichia coli* (*E. coli*) were operated according to the previous report [37]. Briefly, *E. coli* suspension was adjusted with OD600 to be 0.1 by using 2 mM sodium bicarbonate buffer. Then, a volume of 1 mL of 5×10^{-3} mM NOF was mixed with 2 mL of diluted *E. coli* solution, and incubated for 6 h. After the incubation, the mixture was centrifuged to remove the supernatant in tube. A volume of 0.5 mL of the thawed stock 3-(4,5-dimethylthiazol-2-yl)-2,5-diphenyl tetrazolium bromide (MTT) solution was added to the sample and kept at 37 °C for 1 h. Then acid-isopropanol (3 mL isopropanol with 0.04 M HCl) was added and mixed thoroughly, and kept at room temperature for 2 h to ensure that all of the dark blue crystals were dissolved. The absorbance was measured at a wavelength of 570 nm using a UV–vis spectrophotometer.

$$\text{Inhibition\%} = \frac{(A_0 - A)}{A_0} \times 100 \quad (1)$$

where A_0 is the original absorbance of the *E. coli* suspension. A is the absorbance of *E. coli* suspension after incubation. The intermediate solutions of 6.3×10^{-2} mM NOF after reacting with the catalyst and 0.25 mM TX100 under visible light irradiation were sampled at different time intervals, diluted 12.5 times and used for parallel tests instead of NOF. All of the samples were analyzed in triplicate.

3. Results and discussion

3.1. Effect of TX-100 concentration

The photocatalytic degradation of NOF in Bi_2WO_6 dispersions without or with different concentrations of TX100 was initially investigated. As reported in previous studies, the surfactants in aqueous solution can help contaminants be adsorbed on the Bi_2WO_6 surface [28]. It is much easier for those contaminants surrounded by surfactant molecules to reach the Bi_2WO_6 surface to react with the reactive species excited by visible light. The photodegradation of NOF with Bi_2WO_6 under different TX100 concentrations are shown in Fig. 1a where the former 30 min refers to the 30 min of dark adsorption. A great increase of degradation rate was observed with the help of TX100 at concentrations from

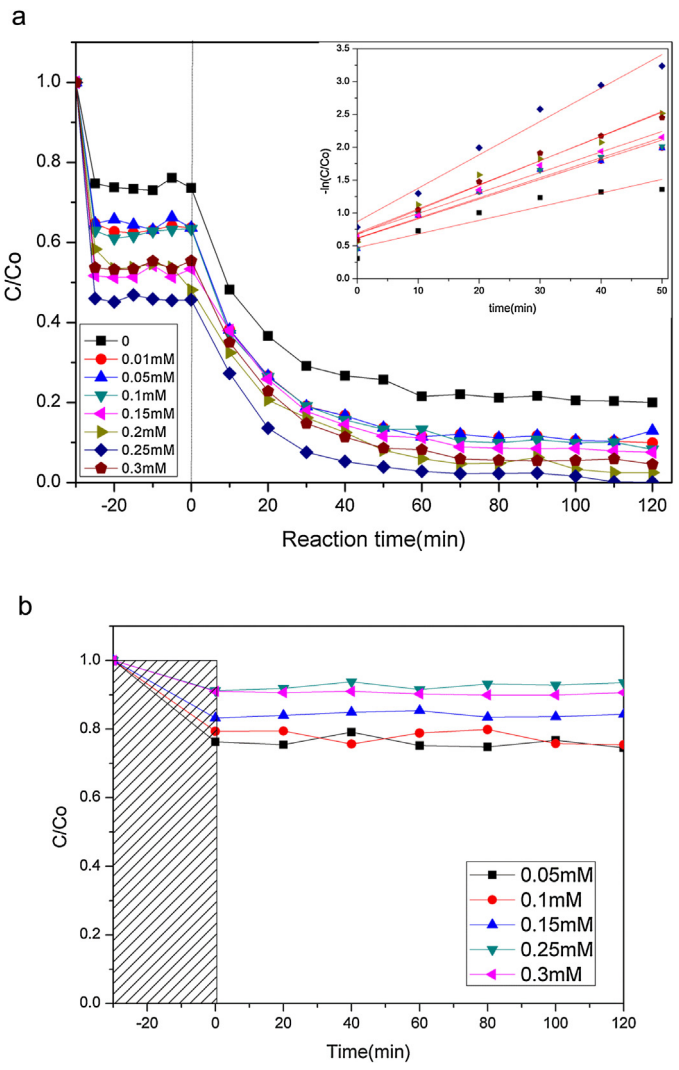

Fig. 1. (a) Photodegradation of NOF with Bi_2WO_6 catalyst under different TX100 concentrations, and first-order fitting curves (inset). (b) Photodegradation of TX100 at different concentrations without NOF by Bi_2WO_6 under visible light irradiation at pH 8.

0.01 mM to 0.25 mM. However, with TX100 concentration increasing to 0.3 mM, slight abatement of NOF degradation occurs. With TX100 at the concentration of 0.25 mM, the removal of NOF is completed within 90 min of irradiation. While only about 79% NOF was degraded by Bi_2WO_6 without TX100 within 120 min. The optical property of TX100/Bi_2WO_6 was analyzed by UV–vis diffuser reflectance. 0.25 mM TX100 had no obvious effect on the optical property of Bi_2WO_6 (shown in Fig. S1).

As reported previously in most similar experiments, the kinetic data of photodegradation of NOF were well fitted by the pseudo-first-order kinetic law described by the equation:

$$-\ln\left(\frac{C}{C_0}\right) = kt \quad (2)$$

where C_0 and C are the NOF concentrations at time zero and t, respectively, and k is the rate constant. All correlation coefficients (R^2) ≥ 0.85. With the addition of TX100, k for NOF degradation was significantly increased (Table 1). It can be found that the decomposition rate of NOF in TX100/Bi_2WO_6 dispersion at 0.25 mM $C_{TX\text{-}100}$ was the highest, which is 25.8 times higher than that without TX100.

The photodegradation of TX100 at different concentrations without NOF by Bi_2WO_6 was also investigated (Fig. 1b). It can

Table 1
Kinetic parameters of the pseudo-first-order model of NOF degradation at virious TX100 concentration.

Sample	TX-100 (0 mM)	TX-100 (0.01 mM)	TX-100 (0.05 mM)	TX-100 (0.1 mM)	TX-100 (0.15 mM)	TX-100 (0.2 mM)	TX-100 (0.25 mM)	TX-100 (0.3 mM)
k	0.016	0.023	0.024	0.024	0.025	0.034	0.043	0.031
R^2	0.85	0.90	0.89	0.91	0.94	0.98	0.96	0.96

be seen that TX100 concentration was reduced during the dark adsorption, but kept stable under visible light irradiation, and scarcely degraded by Bi_2WO_6 photocatalysis. This is probably because that the reactive oxygen species, such as O^{2-}—, HO—, could not break the C—O and CC bonds of TX100. Herein, TX100 was obviously favorable to adsorption and biodegradation process of the poorly soluble hydrophobic pollutant NOF by Bi_2WO_6.

In order to further investigate the above-mentioned effects, a more complex behavior exhibited by TX100 in the bulk solution and on the semiconductor–solution interface has to be carefully examined. The molecular structures of TX100 and NOF and the proposed mechanism of the enhanced adsorption of NOF on Bi_2WO_6 surface in TX100 system is given in Scheme 1. In an aqueous solution, surfactant monomers start aggregating to form micelles at its critical micelle concentration (CMC). The CMC of the TX100 solution was 0.25 mM, shown in Fig. 2. Below the CMC concentration, TX100 present in the bulk solution and on solid–water interface was in monomeric form. The semiconductor surface combining with TX100 through hydrophilic reaction provided strong capturing ability for the target NOF among the incorporated layers. The bulky aromatic moiety of NOF with type π–π binding in the nonionic TX100 molecules could easily and strongly interact with the hydrophilic groups on the Bi_2WO_6 surface, such as the O—H functional bonds [38]. Consequently, the more TX100 monomers incorporated on the surface, the more NOF could be implanted in the space among TX100 monomers close to the hydrophobic terminations. What is more, π–π binding facilitates electron transfer from semiconductor surface to NOF, which improves the photocatalytic degradation of NOF [39]. Hence, the degradation efficiency increased with the increasing amount of surfactant molecules adsorbed, and more NOF can be photodegraded. However, with further increase of the surfactant concentration above CMC, the degradation efficiency decreased. It might be contributed to the NOF incorporated in dense micelles could not contact with the semiconductor surface, thereby decreasing the degradation efficiency.

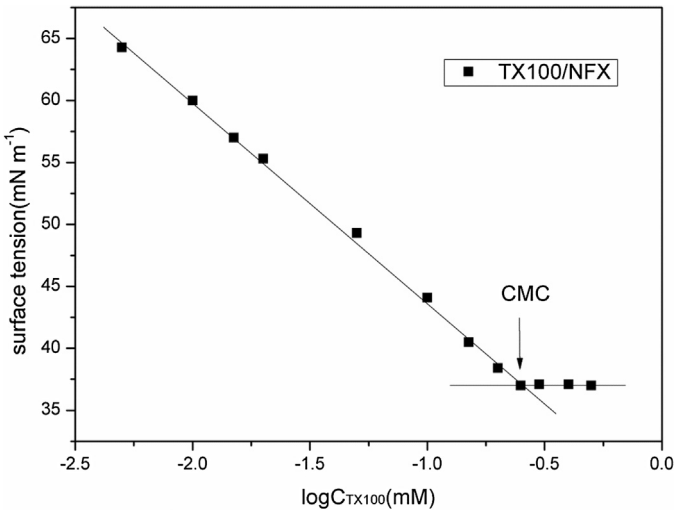

Fig. 2. Variations in the surface tension as a function of the logarithm of the TX100concentration at 25 °C in the presence of Bi_2WO_6.

We conducted the photocatalytic degradation test of NOF by 0.25 mM TX100 under the same conditions without catalyst, shown in Fig. S3. The results showed almost no degradation of NOF by TX100 within 120 min. In general, π–π interaction between aromatic rings is a type of non-covalent interaction, which will not decompose the NOF directly under visible light.

3.2. Effect of pH

Influence of pH varying from 3.96 to 10.1 on the photocatalytic degradation of NOF was also investigated in the aqueous Bi_2WO_6 dispersion in the presence of TX100 at 0.25 mM concentration (Fig. 3a). In such dispersion, about 97% NOF is degraded in 60 min at pH 8.06. While it takes 100 min for 97% NOF to be degraded at pH 3.96. The degradation efficiency of NOF has an

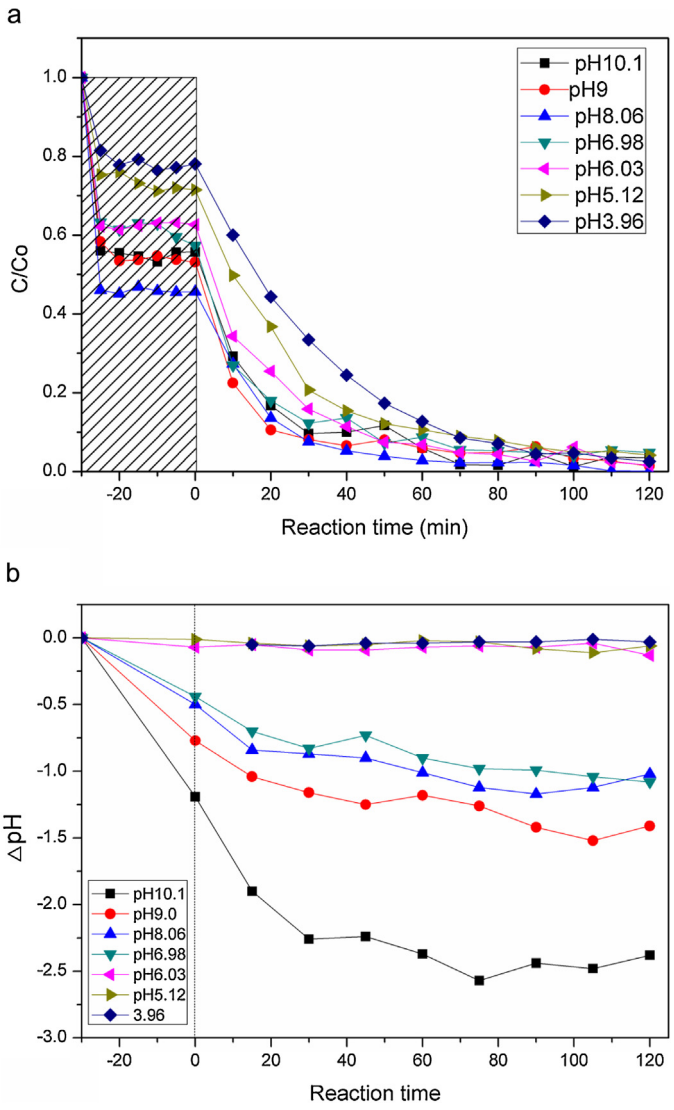

Fig. 3. (a) Effects of pH on the photodegradation of NOF (6.3×10^{-2} mM) in the presence of TX100 at the CMC (0.25 mM). (b) pH variation during reaction ($\triangle pH = pH_t - pH_{initial}$).

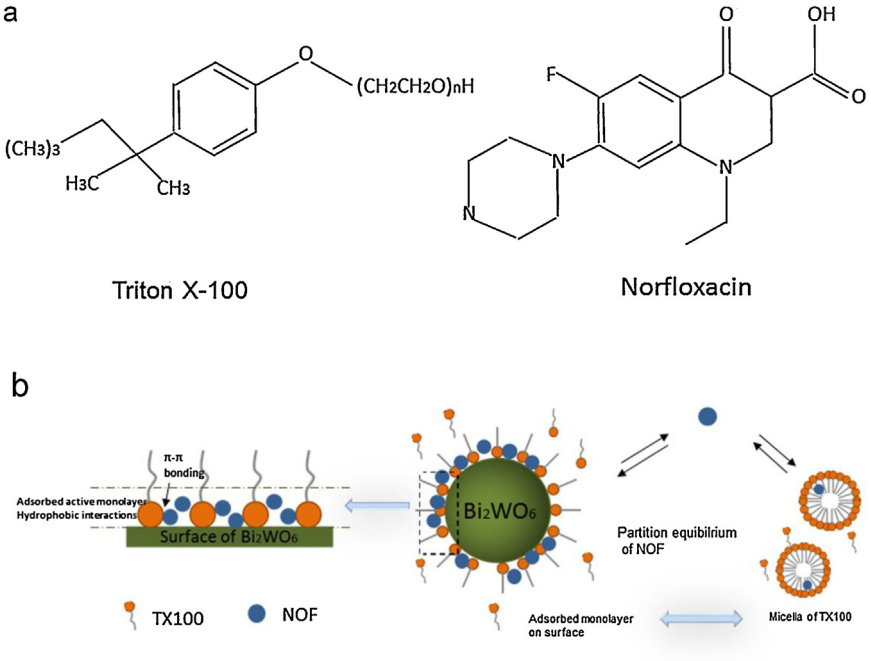

Scheme 1. (a) The molecular structures of TX100 and NOF. (b) The proposed mechanism of the enhanced adsorption of NOF onto Bi_2WO_6 surface in TX100 system.

increasing trend with the pH increasing from 3.96 to 10.1. Such variations in pH can be attributed to the co-adsorption of NOF and TX100 on the Bi_2WO_6 surface, in as much as the adsorption of the nonionic surfactant decreases dramatically at low pH. Adsorption of NOF on Bi_2WO_6 particles is thereby affected. Zhu's group reported that photocatalytic degradation rates of pesticide pyridaben increased with the decrease of pH value due to the surface charge variations of pyridaben adsorbed onto TiO_2 particles [40]. Different from their results, the adsorption of NOF on the Bi_2WO_6 particles is higher in alkaline condition in our study. It might be because NOF was protonated at low pH, and its ionic characteristics led to less solubilization of the NOF in the hydrophobic micelles. At higher pH (above pK_a value), NOF was deprotonated and it behaves like a hydrophobic molecule and easily got solubilized in the micelles [41]. Liu et al. [42] suggested that the adsorption behavior of the nonionic TX100 by the electric attractions on the weakly charged surface of the catalyst was very insignificant at weak acidic conditions. The fast photodegradation occurred in photo irradiation part in alkaline condition because hydroxyl ion could react with photogenerated hole to produce more hydroxyl radical, i.e., Bi_2WO_6 (h^+) + OH^- → •OH + Bi_2WO_6; whereas the photodegradation was inhibited when pH was higher than 10.

In order to further explain the complex effect of pH on the photocatalytic degradation of NOF, the pH variation during photocatalytic reaction was also investigated shown in Fig. 3b. It is noted that an obvious pH decrease occurs during process of photocatalytic reaction especially at pH 10.1 and 9. It suggests that many hydroxyl ions were consumed during the photocatalytic reaction which was consisted with the above mentioned reaction equation. There is a gradual pH drop during the photocatalytic degradation when the initial pH is 8.06 and 6.98. It implies that a continuous consumption of OH^- occurs in the photocatalytic process as well.

3.3. Effect of inorganic ions

Many researchers found that the inorganic salts existing in water showed a significant influence on photocatalytic treatment of pollutants [43,44]. In this study, the effect of selected anions (SO_4^{2-}, HCO_3^-, and NO_3^-) and cationic ions (K^+, Ca^{2+}, Mg^{2+}, and Cu^{2+}) were investigated.

Fig. 4a shows the effects of different anions on the photocatalytic degradation of NOF, and the results showed that both SO_4^{2-} and HCO_3^- retarded the NOF decay rate, according to the equations given in the previous literature:

$$SO_4^{2-} + {}^{\bullet}OH + H^+ \rightarrow {}^{\bullet}SO_4^- + H_2O \quad (3)$$

$$HCO_3^- + {}^{\bullet}OH \rightarrow CO_3^{\bullet-} + H_2O \quad (4)$$

In the above reactions, SO_4^{2-} and HCO_3^- acted as the scavenger of •OH radicals, and meanwhile sulfate radicals ($^{\bullet}SO_4^-$) and carbonate radicals ($CO_3^{\bullet-}$) were formed with continuous consumption of •OH radical. Especially, weaker oxidizing agent sulfate radical formed by SO_4^{2-} reacting with •OH performed a selective oxidation and had a larger molecular structure (than •OH), which might hinder its reaction with the target compounds. In addition, it took a longer time for the sulfate radical than •OH to react with the target NOF in theory, thus retarding the NOF decay in the presence of SO_4^{2-}. However, NO_3^- did not show significant inhibition to the photodegradation of NOF.

The commonly existing inorganic cations, such as K^+, Ca^{2+}, Mg^{2+}, and Cu^{2+}, in natural water were also evaluated. Most inorganic cations are in the highest and stable oxidation state in aquatic environment [45]. It is supposed that these metal ions would have a significant influence on the photodegradation of contaminants in aqueous solution, since they will change the intrinsic viscoelastic properties of the monolayer of nonionic and ionic surfactants at the interface between solid surface and bulk solution [46]. As the intrinsic viscoelastic properties of the monolayer changed, the adsorption of contaminants was thereby affected. As shown in Fig. 4b, all the metal ions display inhibition effects in photocatalytic degradation of NOF. K^+, Ca^{2+}, and Mg^{2+} show a slight influence. This could be attributed to that the intrinsic viscoelastic properties of TX100 monolayer were affected by the presence of these salts, therefore CMC was influenced. The adsorption of NOF on Bi_2WO_6 particles greatly depends on the CMC in the dispersion. How the salts in surfactant solution particularly affect surfactant adsorption on Bi_2WO_6 particles needs to be further investigated.

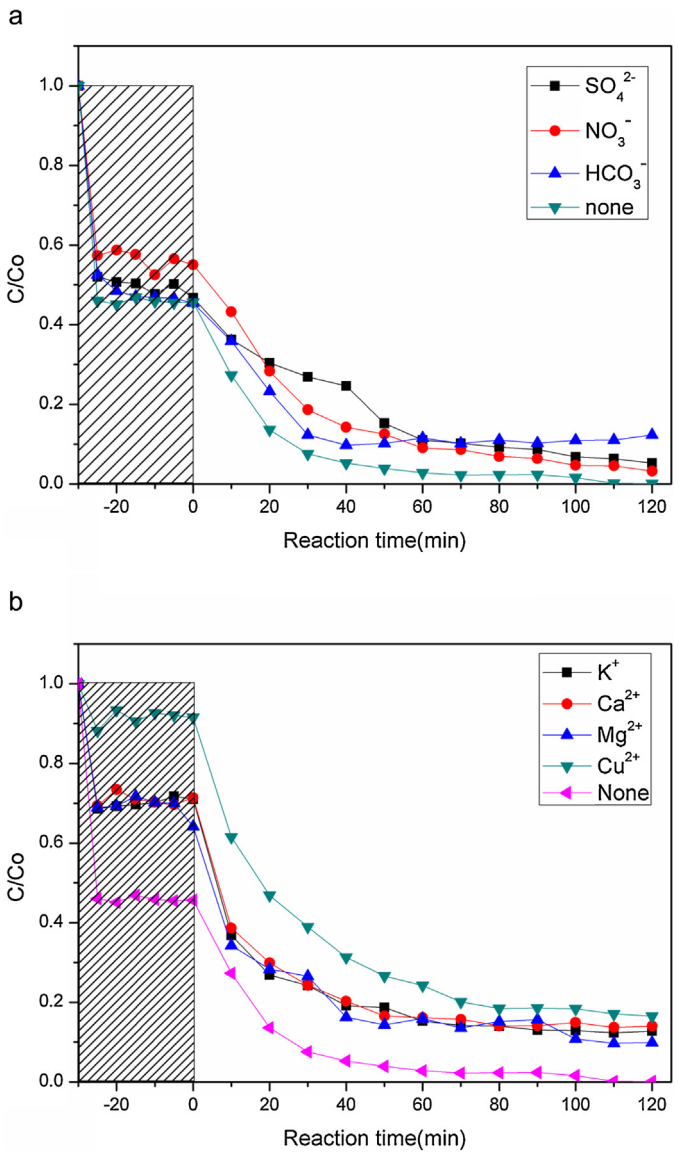

Fig. 4. Effects of (a) inorganic anions (SO_4^{2-}, HCO_3^-, NO_3^-) and (b) inorganic cations (K^+, Ca^{2+}, Mg^{2+}, Cu^{2+}) on the photodegradation of NOF. The concentation of each ion is 10 mM.

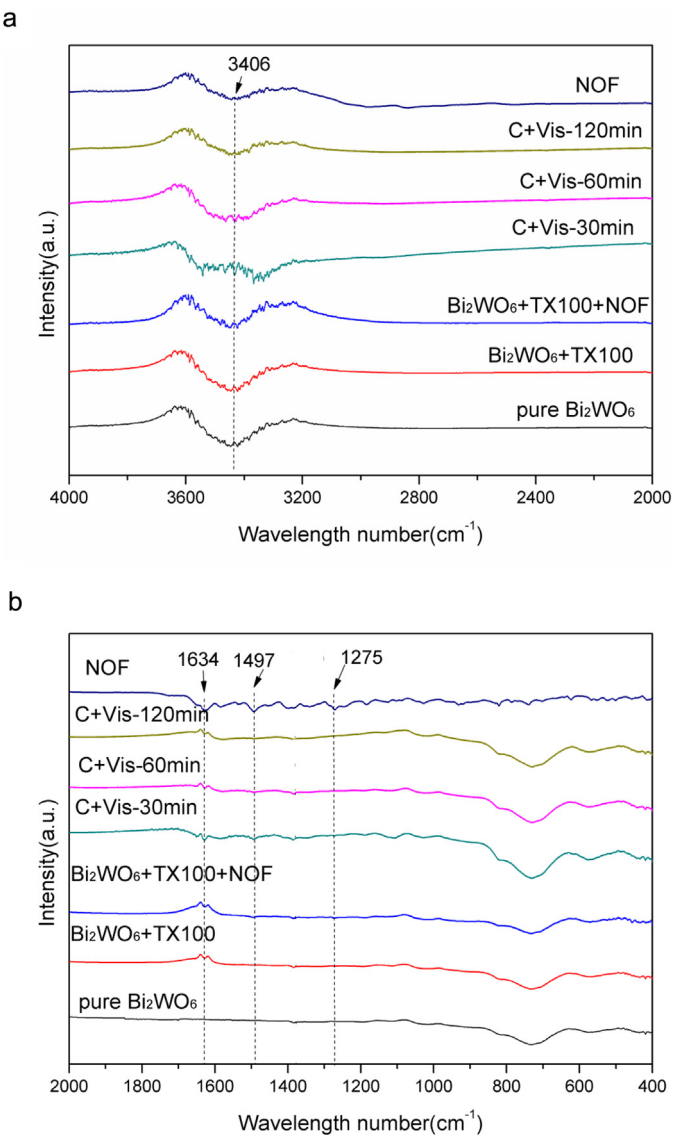

Fig. 5. FT-IR spectra of Bi_2WO_6 after adsorption but without irradiation, irradiation for 0.5 h, 1 h and 1.5 h, pure Bi_2WO_6 and NOF. (a) wavelength from 4000 to 2000 cm^{-1}, (b) wavelength from 2000 to 400 cm^{-1}.

Different from K^+, Ca^{2+} and Mg^{2+}, Cu^{2+} (10 mM) significantly suppressed the photocatalytic degradation of NOF in the reaction solution (Fig. 4b). Cu^{2+} also have an great influence on adsorption of NOF probably because Cu^{2+} react with TX100 to form Cu-chelate which results in drastical decrease of the TX100 concentration in solution. It was reported that Cu^{2+} enhanced the photocatalytic degradation of dimethoate at lower concentration, while inhibited it at higher concentration [47]. In the photodegradation system, •OH radical is the main oxidizing species [48,49]. As mentioned above, Bi_2WO_6 (h^+) + OH^- → •OH + Bi_2WO_6. Photogenerated hole is the key to form •OH radical. In the present study, the photodegradation of NOF by Bi_2WO_6 was inhibited by Cu^{2+} at 10 mM. Hu et al. [50] reported that Cu^{2+} can accept the photoelectrons generated by irradiated catalyst according to the reactions given as follows:

$$Cu^{2+} + e^- \rightarrow Cu^+ + e^- \rightarrow Cu \quad (5)$$

$$Cu + h^+ \rightarrow Cu^+ + h^+ \rightarrow Cu^{2+} \quad (6)$$

At higher Cu^{2+} concentration, Cu^{2+} may compete with OH^- for the photogenerated holes on catalyst surface. Besides, Cu^{2+} might be adsorbed onto Bi_2WO_6 surface. Hence, Cu^{2+} inhibited the degradation by Bi_2WO_6 and higher concentration of Cu^{2+} ions would result in stronger negative effect for NOF degradation. Further study is necessary for elucidating the inherent mechanisms.

3.4. FTIR spectra

Fig. 5a and b illustrates the FTIR spectra of Bi_2WO_6 and its second derivatives after adsorbing NOF at the wavenumber range of 3500–400 cm^{-1}. The main band of Bi_2WO_6 at 3406 cm^{-1} attributed to the OH stretching vibration of —OH in lattice water [51]. After adsorption of TX100, a new peak at 1634 cm^{-1} occurred and corresponded to the weak C=C vibration from bending aromatic groups. After adsorption of NOF, the spectrum of Bi_2WO_6 changed. New peaks appeared in the region of 1000–1500 cm^{-1} attributed to the adsorption of NOF. Compared with the FTIR spectrum of NOF, it is obvious that new peaks of Bi_2WO_6 with NOF adsorbed corresponded to the stretching vibration of bonds in NOF.

The bands at around 1497 and 1275 cm^{-1} corresponded to the asymmetric and symmetric stretching frequencies of the CH_2 and

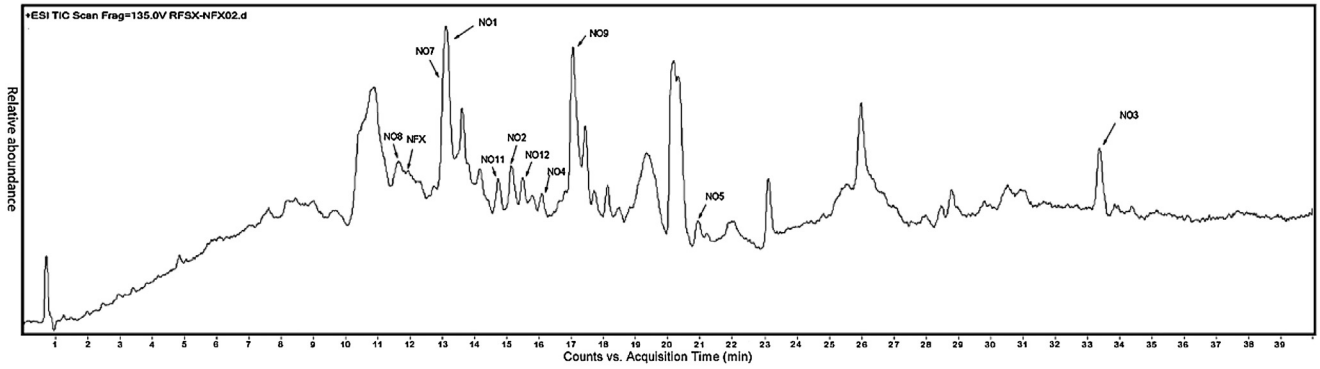

Fig. 6. Total ion chromatogram of photocatalytic degradation products of NOF over Bi_2WO_6. The dosage of Bi_2WO_6 is 1 g/L and the initial pH value is around 8.06, with TX100 (0.25 mM).

O—H bending vibration [52], respectively. C is used to represent Bi_2WO_6 + TX100 + NOF. The spectra of the Bi_2WO_6 after the adsorption of NOF in TX00 solution and after degradation for 30 min were similar to each other, implying that adsorbed substance on the surface was still NOF after irradiation for 30 min. However, after irradiation for 1 and 2 h, the spectra changed distinctly with the disappearance of the peaks at 1250–1300 cm^{-1} and 1450–1500 cm^{-1}, which corresponded to O—H amine stretching vibration and CH_2 deformation vibration, respectively [52]. The disappearance of these two peaks indicates that the adsorbed NOF was degraded and transformed to some intermediate products through losing the —COOH and quinolone structure.

The crystalline phases of Bi_2WO_6 before and after photoreaction with NOF were also characterized by XRD. It can be seen that there is no change of the crystalline phase after reaction, shown in Fig. S2.

Table 2
The information of the intermediates.

Compouds	*m*/*z*	Proposed structure	Compouds	*m*/*z*	Proposed structure
NO2	320	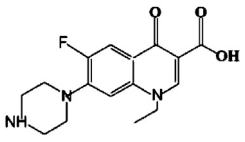	NO7	318	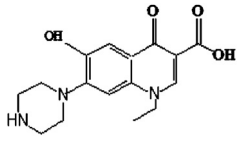
NO1	336	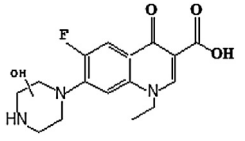	NO8	334	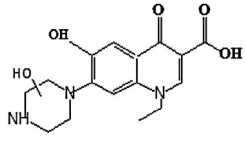
NO2	350	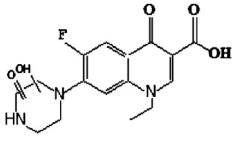	NO9	306	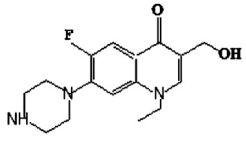
NO3	338	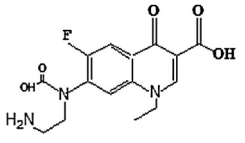	NO10	296	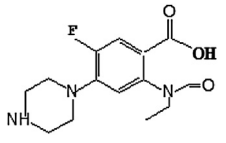
NO4	294	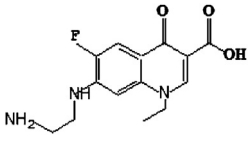	NO11	270	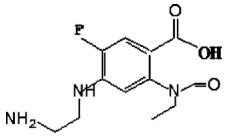
NO5	279	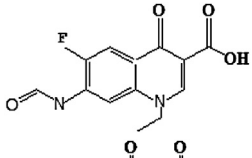	NO12	227	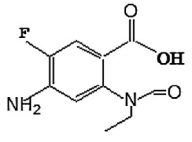
NO6	251	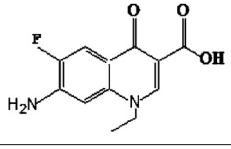			

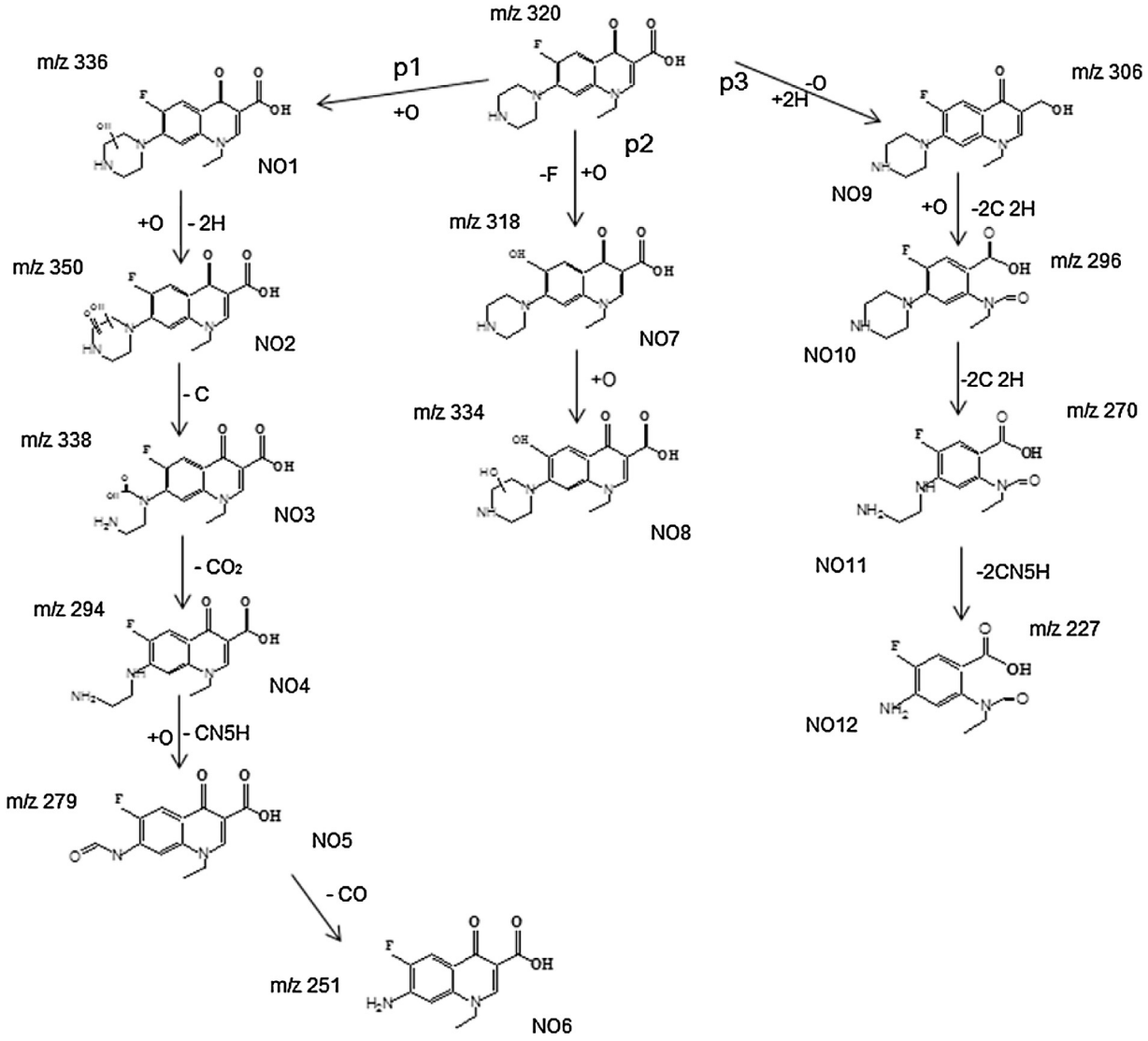

Fig. 7. Possible photocatalytic degradation ways of NOF after irradiation over Bi_2WO_6.

3.5. Photocatalytic degradation intermediates and possible degradation pathways for NOF

The main photodegradation intermediates were also identified by HPLC and LC/MS/MS to determine the reaction mechanism along the route to photodegradation. In regard to determination of the photodegradation products during Bi_2WO_6 treatment process of NOF, all mass spectrogram of main intermediates are given in Fig. 6. No intermediate was detected by LC/MS/MS during the adsorption process. However, twelve intermediates were identified in the Bi_2WO_6 irradiated process. The molecular weights of the intermediates and proposed molecular structure are summarized in Table 2. Spectrum of all intermediates are given from Fig. S4 to Fig. S11. Best choice of the chemical structure is in the light of prior knowledge of the molecule pattern. Previous research found the products with *m*/*z* of 322, 336, 294 and 251 [32], due to partial elimination of the piperazine ring. These main products were also found in this work, but the *m*/*z* 251 was found only in a small amount, and the product with *m*/*z* of 306 was firstly found due to the losing of oxygen atoms in the carboxy group. The intermediate NO7 with *m*/*z* 318 was attributed to the F atom replacement by hydroxyl ion. The cleaved fragments with *m*/*z* $[M+H-14]^+$ and $[M+H-26]^+$ were attributed to the loss of oxygen atoms and $-CH_2-CH_2$, generating intermediates *m*/*z* 306 and 294, respectively.

According to the intermediate determination, the photocatalytic degradation of NOF was supposed to be mainly composed by three pathways, including piperazine ring transformation (pathway1), defluorination (pathway 2), and decarboxylation (pathway 3) (Fig. 7). In pathway 1, hydroxyl keto-derivative (NO2; *m*/*z* 350) is obtained by an additional step of incorporation of an oxygen atom. Subsequent loss of CO results in opening of the piperazinyl ring (NO3; *m*/*z* 294), following by the structure rearrangement and the generation of amide (with NH—CH=O group). Similar reaction between piperazine ring and •OH radicals in TiO_2 photocatalysis has been reported [32], and the products with *m*/*z* of 336 and 350 were detected in TiO_2 photocatalysis. The generation of NO4 (*m*/*z* 294) can be ascribed to the loss of CO_2 in NO3 with functional group of —NH—COOH. The further •OH oxidation of NO4 led to the further decarbonylation and the generation of NO5. From NO4 to NO6, the amine with functional group of $-NH-CH_2-CH_2-NH_2$ (NO4) was oxidized to amide —NH—CH=O (NO5) and then decarbonylated to amine NH_2 (NO6). This is consistent with FTIR characterization that the disappearance of peaks at 1450–1500 cm^{-1} due to loss of the $-CH_2-CH_2$. Compared to oxidation of the piperazine ring of NOF, the occurrence of NO7 with *m*/*z* 318 reveals the further oxidation of

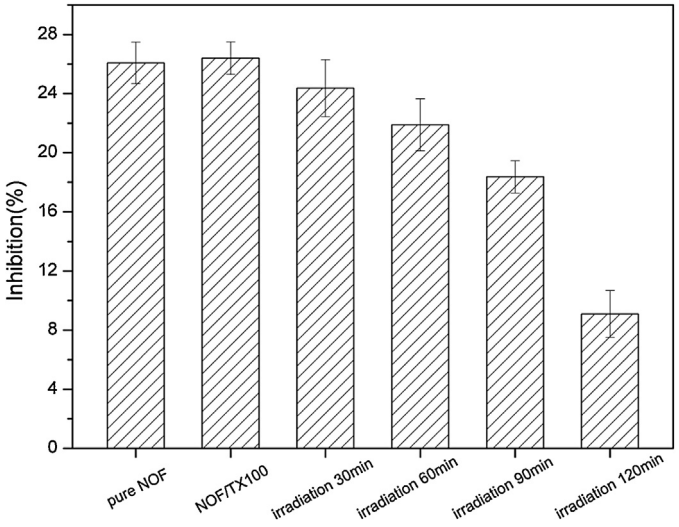

Fig. 8. The toxicity evaluation of NOF and the reaction solutions at different time intervals under visible light irradiation. The original NOF concentration is 6.3×10^{-2} mM, Bi_2WO_6 dosage is 1.0 g/L, and TX100 concentration is 0.25 mM. The reaction solution was diluted 12.5 times for toxicity test.

fluorine atom at the benzene ring which is substituted by hydroxyl (shown in pathway 2). NO7 was obtained from the hydroxyl oxidation at the carbon of piperazine, while no keto-derivative products with m/z 348 were found. Compared to the main degradation route pathway 1, pathway 2 is an alternative pathway, which did not completely break the piperazine ring. The possible reason needs to be further studied. Another degradation step was decarboxylation of the carboxyl group to form NO9 (m/z 306) in the pathway 3. This hypothesis is consistent with previous publications [53]. Four structures NO9, NO10, NO11, and NO12 with m/z of 306, 296, 270, and 227, respectively, were obtained from decarboxylation and opening piperazine ring.

In conclusion, the photocatalysis degradation of NOF occurs at least at two functional sections of the molecule, the piperazinyl substituent and, the quinolone moiety. Three reaction pathways were proposed, which differs from others previously reported in the literature although with some analogous degradation parts [49]. The decarboxylation here was revealed to be transformation of —COOH to —CH_2—OH, different from the pathway reported previous literatures [32,54]. NO11 and NO12 were first reported. Besides, further piperazine oxidation was not observed in the degradation pathway 2. Other degradation pathways might also exist but were not found in this work.

In order to estimate the reusability of the catalyst in practical application, the catalyst was washed by 1 M HCl after each photodegradation process for five successive cycles. According to the results, the photodegradation efficiency slightly decreased with the increasing cycles, but was still over 80% after the five cycles, higher than the original photocatalytical degradation efficiency with only Bi_2WO_6. The reduction of degradation efficiency after each cycle can be explained by the loss of catalyst during the washing step [55]. This indicates that this method can be reused effectively in photodegradation process.

3.6. Toxicity evaluation

The toxicity evaluation results are shown in Fig. 8. NOF is a fluoroquinolone antibiotic and have antibacterial effect, possessing high antibacterial activity especially for aerobic gram-negative bacilli, such as *E. coli*. The inhibition of *E. coli* activity by NOF was 26%. And the added TX100 has almost no obvious inhibition of *E. coli* activity. As the reaction of the same amount of NOF with the catalyst went on, its inhibition of *E. coli* activity decreased gradually to lower than 10%, indicating the toxicity of the reaction intermediates is much lower than NOF.

4. Conclusion

Amphipathic nonionic surfactant TX100 added to Bi_2WO_6 aqueous solution is greatly in favor of adsorption and photodegradation of NOF. The adsorption of NOF on the Bi_2WO_6 surface is significantly enhanced by TX100 during photocatalytic degradation process. The degradation kinetics of NOF followed pseudo-first-order equation. The surfactant monomer adsorbed on the Bi_2WO_6 surface could provide a nonaqueous "cage" leading to a higher degradation, but with more than 0.25 mM of TX100, the degradation efficiency lowered. In the alkaline solution, the degradation rate of NOF was higher than that in the acidic one, because alkaline media facilitates the adsorption of TX100, and higher concentration of hydroxyl ions in alkaline media could react with the holes to form hydroxyl radicals. The effect of inorganic ions of SO_4^-, HCO_3^-, and Cu^{2+} on the $^{\bullet}OH$ and h^+ during photocatalytic degradation process was further confirmed. It can be confirmed that the photocatalytic degradation of NOF was mainly influenced by hydroxyl radicals and the separation of photogenerated electrons and holes. FTIR analyses demonstrated that the adsorbed NOF was completely degraded after 2 h irradiation. According to the HPLC/MS/MS analysis, three possible pathways of the photocatalytic degradation of NOF were proposed, including piperazine ring transformation, defluorination, and decarboxylation. The toxicity of the reaction intermediates are less toxical than NOF. We have reasons to believe that photocatalysis under visible light irradiation treatment with the help of TX100 is an attractive method in treatment of antibiotics contamination which are poorly soluble in water.

Acknowledgements

The study was financially supported by the National Program for Support of Top-Notch Young Professionals of China (2012), the National Natural Science Foundation of China (51222805), the Program for New Century Excellent Talents in University from the Ministry of Education of China (NCET-11-0129), the Fundamental Research Funds for the Central Universities, Hunan University.

Appendix A. Supplementary data

Supplementary data associated with this article can be found, in the online version, at http://dx.doi.org/10.1016/j.jhazmat.2015.12.044.

References

[1] R. Hirsch, T. Ternes, K. Haberer, K.L. Kratz, Occurrence of antibiotics in the aquatic environment, Sci. Total Environ. 225 (1999) 109–118.
[2] K. Oberleí, M.J. Capdeville, T. Berthe, H.L. Budzinski, F. Petit, Evidence for a complex relationship between antibiotics and antibiotic-resistant *E. coli*: from medical center patients to a receiving environment, Environ. Sci. Technol. 46 (2012) 1859–1868.
[3] K. Kümmerer, Resistance in the environment, J. Antimicrob. Chemother. 54 (2004) 311–320.
[4] S. Simoens, J. Verhaegen, P. Van Bleyenbergh, W.E. Peetermans, M. Decramer, Consumption patterns and in vitro resistance of *Streptococcus pneumoniae* to fluoroquinolones, Antimicrob. Agents Chemother. 55 (2011) 3051–3053.
[5] Z. Yu, S. Peldszus, P.M. Huck, Adsorption characteristics of se lected pharmaceuticals and an endocrine disrupting compound – naproxen, carbamazepine and nonylphenol – on activated carbon, Water Res. 42 (2008) 2873–2882.
[6] K. Ikehata, N. Jodeiri Naghashkar, M. Gamal El-Din, Degradation of aqueous pharmaceuticals by ozonation and advanced oxidation processes: a review, Ozone Sci. Eng. 28 (2006) 353–414.

[7] C. Zwiener, S. Seeger, T. Glauner, F. Frimmel, Metabolites from the biodegradation of pharmaceutical residues of ibuprofen in biofilm reactors and batch experiments, Anal. Bioanal. Chem. 372 (2002) 569–575.
[8] L. Tang, S. Zhang, G.M. Zeng, Rapid adsorption of 2,4-dichlorophenoxyacetic acid by iron oxide nanoparticles-doped carboxylic ordered mesoporous carbon, J. Colloid Interface Sci. 445 (2015) 1–8.
[9] G. Yang, L. Tang, Y. Cai, Effective removal of Cr (VI) through adsorption and reduction by magnetic mesoporous carbon incorporated with polyaniline, RSC Adv. 102 (2014) 58362–58371.
[10] L. Tang, Y. Fang, Y. Pang, Synergistic adsorption and reduction of hexavalent chromium using highly uniform polyaniline–magnetic mesoporous silica composite, Chem. Eng. J. 254 (2014) 302–312.
[11] Y. Liu, G. Zeng, L. Tang, et al., Highly effective adsorption of cationic and anionic dyes on magnetic Fe/Ni nanoparticles doped bimodal mesoporous carbon, J. Colloid Interface Sci. 448 (2015) 451–459.
[12] T.E. Doll, F.H. Frimmel, Cross-flow microfiltration with periodical back-washing for photocatalytic degradation of pharmaceutical and diagnostic residues—evaluation of the long-term stability of the photocatalytic activity of TiO_2, Water Res. 39 (2005) 847–854.
[13] H. Fu, C. Pan, W. Yao, Y. Zhu, Visible-light-induced degradation of rhodamine B by nanosized Bi_2WO_6, J. Phys. Chem. B 109 (2005) 22432–22439.
[14] L. Zhang, W. Wang, Z. Chen, L. Zhou, H. Xu, W. Zhu, Fabrication of flower-like Bi_2WO_6 superstructures as high performance visible-light driven photocatalysts, J. Mater. Chem. 17 (2007) 2526–2532.
[15] N. Tian, Y. Zhang, H. Huang, Influences of Gd substitution on the crystal structure and visible-light-driven photocatalytic performance of Bi_2WO_6, J. Phys. Chem. C 29 (2014) 15640–15648.
[16] H. Huang, K. Liu, K. Chen, Ce and F comodification on the crystal structure and enhanced photocatalytic activity of Bi_2WO_6 photocatalyst under visible light irradiation, J. Phys. Chem. C 26 (2014) 14379–14387.
[17] M. Chen, W. Chu, Efficient degradation of an antibiotic norfloxacin in aqueous solution via a simulated solar-light-mediated Bi_2WO_6 process, Ind. Eng. Chem. Res. 51 (2012) 4887–4893.
[18] Y. Fu, C. Chang, P. Chen, Enhanced photocatalytic performance of boron doped Bi_2WO_6 nanosheets under simulated solar light irradiation, J. Hazard. Mater. 254 (2013) 185–192.
[19] Z. Zhang, W. Wang, E. Gao, Enhanced photocatalytic activity of Bi_2WO_6 with oxygen vacancies by zirconium doping, J. Hazard. Mater. 196 (2011) 255–262.
[20] J. Di, J. Xia, Y. Ge, Novel visible-light-driven CQDs/Bi_2WO_6 hybrid materials with enhanced photocatalytic activity toward organic pollutants degradation and mechanism insight, Appl. Catal. B 168 (2015) 51–61.
[21] Y. Liang, S. Lin, L. Liu, Oil-in-water self-assembled Ag@ AgCl QDs sensitized Bi_2WO_6: enhanced photocatalytic degradation under visible light irradiation, Appl. Catal. B 164 (2015) 192–203.
[22] H. Hidaka, S. Yamada, S. Suenaga, J. Zhao, N. Serpone, E. Pelizzetti, Photodegradation of surfactants: part VI complete photocatalytic degradation of anionic, cationic and nonionic surfactants in aqueous semiconductor dispersions, J. Mol. Catal. 59 (1990) 279–290.
[23] E. Pramauro, A.B. Prevot, M. Vincenti, R. Gamberini, Photocatalytic degradation of naphthalene in aqueous TiO_2 dispersions: effect of nonionic surfactants, Chemosphere 36 (1998) 1523–1542.
[24] A.B. Prevot, E. Pramauro, M. de la Guardian, Photocatalytic degradation of carbaryl in aqueous TiO_2 suspensions containing surfactants, Chemosphere 39 (1999) 493–502.
[25] K. Yang, L. Zhu, B. Xing, Enhanced soil washing of phenanthrene by mixed solutions of TX100 and SDBS, Environ. Sci. Technol. 40 (2006) 4274–4280.
[26] Y. Zhang, H. Wu, J. Zhang, H. Wang, W. Lu, Enhanced photodegradation of pentachlorophenol by single and mixed cationic and nonionic surfactants, J. Hazard. Mater. 221 (2012) 92–99.
[27] H. Hidaka, J. Hiroyuki, K. Nohara, J. Zhao, Photocatalytic degradation of the hydrophobic pesticide permethrin in fluoro surfactant/TiO_2 aqueous dispersions, Chemosphere 25 (1992) 1589–1597.
[28] T. Wu, G. Liu, J. Zhao, H. Hidaka, N. Serpone, Photoassisted degradation of dye pollutants. V. Self-photosensitized oxidative transformation of rhodamine B under visible light irradiation in aqueous TiO_2 dispersions, J. Phys. Chem. B 102 (1998) 5845–5851.
[29] J. Zhao, T. Wu, K. Wu, K. Oikawa, H. Hidaka, N. Serpone, Photoassisted degradation of dye pollutants. 3. Degradation of the cationic dye rhodamine B in aqueous anionic surfactant/TiO_2 dispersions under visible light irradiation: evidence for the need of substrate adsorption on TiO_2 particles, Environ. Sci. Technol. 32 (1998) 2394–2400.
[30] G.A. Epling, C. Lin, Photoassisted bleaching of dyes utilizing TiO_2 and visible light, Chemosphere 46 (2002) 561–570.
[31] D.J. Pollard, J.M. Woodley, Biocatalysis for pharmaceutical intermediates: the future is now, Trends Biotechnol. 25 (2007) 66–73.
[32] T. An, H. Yang, W. Song, G. Li, H. Luo, W.J. Cooper, Mechanistic considerations for the advanced oxidation treatment of fluoroquinolone pharmaceutical compounds using TiO_2 heterogeneous catalysis, J. Phys. Chem. A 114 (2010) 2569–2575.
[33] J.W. Jawitz, D. Dai, P.S.C. Rao, M.D. Annable, R.D. Rhue, Rate-limited solubilization of multicomponent nonaqueous-phase liquids by flushing with cosolvents and surfactant: modeling data from laboratory and field experiment, Environ. Sci. Technol. 37 (2003) 1983–1991.
[34] M. Teresa Alcántara, Jose Gómez, Marta Pazos, M. Angeles Sanromán, PAHs soil decontamination in two steps: desorption and electrochemical treatment, J. Hazard. Mater. 166 (2009) 462–468.
[35] T. Zordan-Nudo, V. Ling, Z. Liu, Effects of nonionic detergents on *P*-glycoprotein drug binding and reversal of multidrug resistance, Cancer Res. 53 (24) (1993) 5994–6000.
[36] T.G. Van Thienen, K. Raemdonck, J. Demeester, Protein release from biodegradable dextran nanogels, Langmuir 23 (19) (2007) 9794–9801.
[37] H. Wang, H. Cheng, F. Wang, An improved 3-(4,5-dimethylthiazol-2-yl)-2,5-diphenyl tetrazolium bromide (MTT) reduction assay for evaluating the viability of *E. coli* cells, J. Microbiol. Method 82 (2010) 330–333.
[38] I. Ramakanth, A. Patnaik, Characteristics of solubilization and encapsulation of fullerene C60 in non-ionic Triton X-100 micelles, Carbon 46 (2008) 692–698.
[39] A. Takai, M. Chkounda, A. Eggenspiller, C.P. Gros, M. Lachkar, J.-M. Barbe, S. Fukuzumi, Efficient photoinduced electron transfer in a porphyrin tripod-fullerene supramolecular complex via π–π interactions in nonpolar media, J. Am. Chem. Soc. 132 (2010) 4477–4489.
[40] X. Zhu, C. Yuan, H. Chen, Photocatalytic degradation of pesticide pyridaben. 3. In surfactant/TiO_2 aqueous dispersions, Environ. Sci. Technol. 41 (2007) 263–269.
[41] M. Purkait, S. DasGupta, S. De, Performance of TX-100 and TX-114 for the separation of chrysoidine dye using cloud point extraction, J. Hazard. Mater. 137 (2006) 827–835.
[42] J. Liu, R. Han, H. Wang, Y. Zhao, Z. Chu, H. Wu, Photoassisted degradation of pentachlorophenol in a simulated soil washing system containing nonionic surfactant Triton X-100 with La–B codoped TiO_2 under visible and solar light irradiation, Appl. Catal. B 103 (2011) 470–478.
[43] M. Sökmen, A. Özkan, Decolourising textile wastewater with modified titania: the effects of inorganic anions on the photocatalysis, J. Photochem. Photobiol. A 147 (2002) 77–81.
[44] C. Guillard, H. Lachheb, A. Houas, M. Ksibi, E. Elaloui, J.-M. Herrmann, Influence of chemical structure of dyes, of pH and of inorganic salts on their photocatalytic degradation by TiO_2 comparison of the efficiency of powder and supported TiO_2, J. Photochem. Photobiol. A 158 (2003) 27–36.
[45] C. Wang, L. Zhu, M. Wei, P. Chen, G. Shan, Photolytic reaction mechanism and impacts of coexisting substances on photodegradation of bisphenol A by Bi_2WO_6 in water, Water Res. 46 (2012) 845–853.
[46] A. Bonfillon, D. Langevin, Viscoelasticity of monolayers at oil–water interfaces, Langmuir 9 (1993) 2172–2177.
[47] J.Q. Chen, Z.J. Hu, D. Wang, C.J. Gao, R. Ji, Photocatalytic mineralization of dimethoate in aqueous solutions using TiO_2: parameters and by-products analysis, Desalination 258 (2010) 28–33.
[48] H. Park, Y. Park, W. Kim, W. Choi, Surface modification of TiO_2 photocatalyst for environmental applications, J. Photochem. Photobiol. C 15 (2013) 1–20.
[49] M.R. Hoffmann, S.T. Martin, W. Choi, D.W. Bahnemann, Environmental applications of semiconductor photocatalysis, Chem. Rev. 95 (1995) 69–96.
[50] C. Hu, C.Y. Jimmy, Z. Hao, P. Wong, Effects of acidity and inorganic ions on the photocatalytic degradation of different azo dyes, Appl. Catal. B 46 (2003) 35–47.
[51] R. Singhal, M. Datta, Development of nanocomposites of bentonite with polyaniline and poly (methacrylic acid), J. Appl. Polym. Sci. 103 (2007) 3299–3306.
[52] S. Sahoo, C.K. Chakraborti, S.C. Mishra, U. Nanda, S. Naik, FTIR and XRD investigations of some fluoroquinolones, Int. J. PharmTech Res. 4 (2012) 382–391.
[53] Pérez-Estrada, S. Malato, W. Gernjak, A. Agüera, E.M. Thurman, I. Ferrer, A.R. Fernández-Alba, Photo-Fenton degradation of diclofenac: identification of main intermediates and degradation pathway, Environ. Sci. Technol. 39 (2005) 8300–8306.
[54] M. Chen, W. Chu, Photocatalytic degradation and decomposition mechanism of fluoroquinolones norfloxacin over bismuth tungstate: experiment and mathematic model, Appl. Catal. B 168–169 (2015) 175–182.
[55] S.M. Lam, J.C. Sin, A.R. Mohamed, Parameter effect on photocatalytic degradation of phenol using TiO_2-P25/activated carbon (AC), Korean J. Chem. Eng. 27 (2010) 1109–1116.